Louis J. Ghosn[1], *Pete Kantzos*[2], *and Jack Telesman*[3]

Fatigue Crack Growth and Crack Bridging in SCS-6/Ti-24-11

REFERENCE: Ghosn, L. J., Kantzos, P., and Telesman, J., "**Fatigue Crack Growth and Crack Bridging in SCS-6/Ti-24-11,**" *Cyclic Deformation, Fracture, and Nondestructive Evaluation of Advanced Materials: Second Volume, ASTM STP 1184*, M. R. Mitchell and O. Buck, Eds., American Society for Testing and Materials, Philadelphia, 1994, pp. 64–86.

ABSTRACT: Interfacial damage induced by relative fiber/matrix sliding was found to occur in the bridged zone of unidirectional SCS-6/Ti-24Al-11Nb intermetallic matrix composite specimens subjected to fatigue crack growth conditions. The degree of interfacial damage was not uniform along the bridged crack wake. Higher damage zones were observed near the machined notch in comparison to the crack tip. The interfacial friction shear strength, τ_i, measured in the crack wake using pushout testing revealed lower values than the as-received interface. Interfacial wear also reduced the strength of the bridging fibers. The reduction in fiber strength is thought to be a function of the magnitude of relative fiber/matrix displacements and the degree of interfacial damage. Furthermore, two different fiber bridging models were used to predict the influence of bridging on the fatigue crack driving force. The shear lag model required a variable τ_i in the crack wake (reflecting the degradation of the interface) before its predictions agreed with trends exhibited by the experimental data. The fiber pressure model did an excellent job in predicting both the FCG data and the ΔCOD in the bridged zone even though it does not require a knowledge of τ_i.

KEYWORDS: intermetallic matrix composites, fatigue crack growth, crack bridging, shear-lag model, fiber pressure model, interfacial shear stress, fiber pushout, effective fatigue driving force, fiber strength, interfacial damage

Intermetallic matrix composites (IMC) are candidate materials for high-temperature aerospace applications where high strength and low weight are required. However, before these composites can be implemented, it is necessary to understand the fatigue crack growth process and the evolution of damage in order to accurately predict the lives of composite components.

An important mechanism influencing fatigue crack growth behavior in IMCs is crack bridging. Fatigue cracks become bridged as the crack propagates in the matrix while leaving the fibers intact in the crack wake. The bridging fibers carry part of the applied load and shield the crack tip. Consequently, crack bridging enhances the fatigue crack growth behavior of IMCs in comparison to their unreinforced matrix alloys. Crack bridging has been widely observed in SCS-6/Ti-based composites under fatigue loading conditions [*1–5*].

The effectiveness of fiber bridging in reducing the crack driving force depends on the inter-

[1] Research engineer, Case Western Reserve University, NASA Lewis Resident Research Associate, Mail Stop 49-7, 21000 Brookpark Rd., Cleveland, OH 44135.

[2] Research engineer, Ohio Aerospace Institute, NASA Lewis Mail stop 49-7, 21000 Brookpark Rd., Cleveland, OH 44135.

[3] Material engineer, NASA Lewis Research Center, Mail Stop 49-7, 21000 Brookpark Rd., Cleveland, OH 44135.

facial properties and fiber strength. If the interface strength is too low, the matrix does not transfer enough load to the bridging fibers to effectively shield the crack tip. On the other hand, a strong interface will limit the extent of fiber/matrix sliding, resulting in high fiber stresses and ultimately fiber failures. Therefore, an optimum interface strength is desired to produce effective crack bridging. Likewise, high-strength fibers will also promote better crack bridging.

The interfacial properties of the bridging fibers may also be influenced by the load history. The interfacial wear induced by fiber/matrix sliding can change the interface properties and fiber strength. Unfortunately, very little is known regarding the degradation of these properties as a function of interfacial wear even though these properties are required input into fiber bridging models such as shear lag [*6–8*]. Preliminary measurements of interfacial shear properties did indeed show a decrease in the frictional shear stress with cyclic loading [*9–11*].

In this report, fiber bridging was studied by performing fatigue crack growth testing on a unidirectional SCS-6/Ti-24Al-11Nb (a%) using single edge notch (SEN) and center crack panel (CCP) specimens in a specially designed fatigue loading stage mounted inside a scanning electron microscope. The evolution of interfacial damage in the tested specimens was investigated by performing fiber pushout tests and fiber tensile tests on specimens previously subjected to crack bridging.

Finally, the effect of fiber bridging on the crack opening displacements and effective crack driving forces was studied analytically using the shear lag and fiber pressure models.

Experimental Procedures

Fatigue Crack Growth Testing

Fatigue crack growth testing of a unidirectional 33% fiber volume fraction SCS-6/Ti-24Al-11Nb composite was performed using SEN and CCP specimens. Both specimen geometries are shown in Fig. 1.

Fatigue crack growth testing was performed using a closed loop servo-hydraulic testing machine specially designed for the scanning electron microscope (SEM) [*12*]. This unique loading stage enables real time in situ observations of the fatigue crack growth process at magnifications up to × 10 000. All specimens were tested at room temperature inside the SEM chamber (1×10^{-6} torr). Test frequencies ranged from 1 to 5 Hz. The load ratio R was 0.1 in all cases. Testing was interrupted regularly in order to record the crack opening displacements at maximum and minimum loads and to measure crack extension. When possible, measurements of crack extension and crack opening displacements were made on both surfaces of the specimen. The complete test matrix is shown in Table 1. The material properties assumed in this study are shown in Table 2.

Debond Length Measurements

In order to observe interfacial damage and attempt to determine the extent of fiber/matrix debonding, interrupted fatigue crack growth specimens were examined nondestructively by scanning acoustic microscopy (SAM) [*13*]. This work was performed by General Electric Aircraft Engines [*14*]. The specimens were also chemically etched (using a nitric/hydrofluoric solution) to remove the matrix and expose the fibers. Measurements of the damaged interface lengths were made at high magnifications in the SEM. The total damage zone observed for every fiber was taken as the debond length and used to determine the interfacial frictional shear strength.

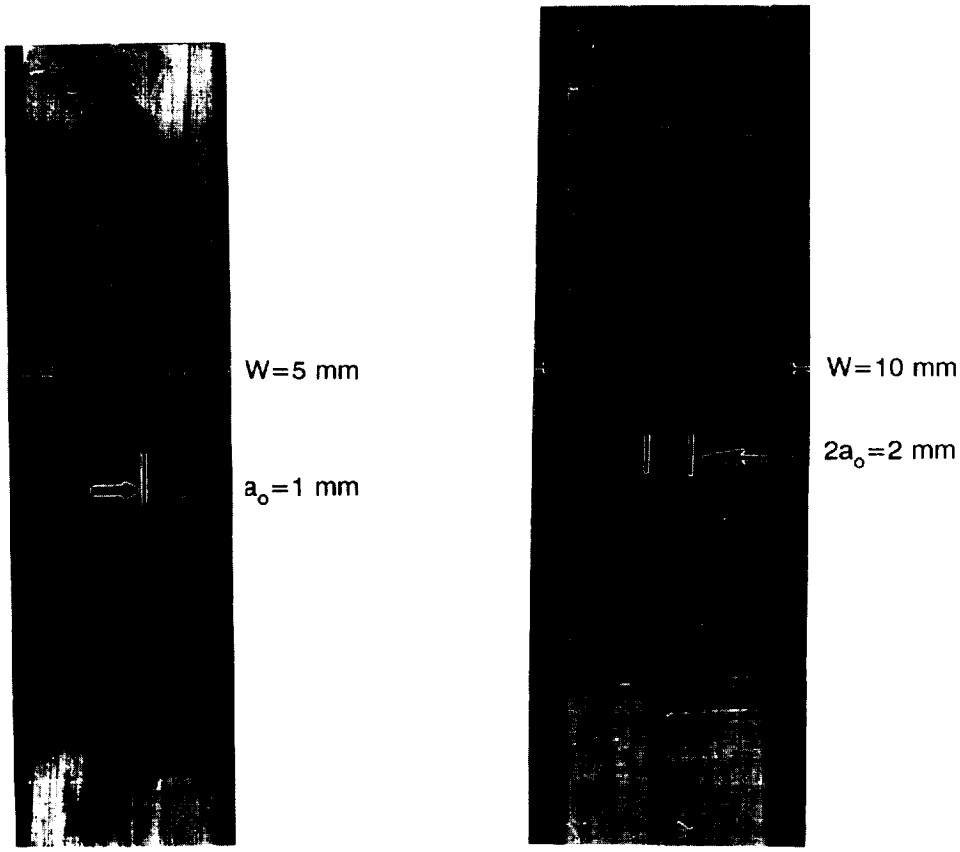

FIG. 1—*Fatigue crack growth specimens:* (a) *single-edge notch (SEN), and* (b) *center crack panel (CCP).*

TABLE 1—*Fatigue crack growth test matrix.*

	Initial Notch, a_o, mm	Width, W, mm	Thickness t, mm	Applied stress $\Delta\sigma = \sigma_{max}$-$\sigma_{min}$, MPa
		SINGLE EDGE NOTCH SPECIMENS		
SEN1[a]	1.054	5.071	1.930	262
SEN2[a]	1.203	5.088	1.860	180, 360
SEN3[a]	1.016	5.085	1.930	180, 248, 276
SEN4[a]	1.031	5.080	1.788	264
SEN5[a]	1.024	5.080	1.753	276
		CENTER CRACK PANEL SPECIMENS		
CCP1	1.015	10.04	0.86	348
CCP2	1.006	9.95	0.89	344
CCP3[a]	1.249	10.14	1.905	228

[a] Heat-treated.

TABLE 2—*SCS-6/Ti-24-11 intermetallic matrix composite properties assumed.*

Composite SCS-6/Ti-24-11			Fiber SCS-6		Matrix Ti-24-11	
Elastic modulus	Transverse, E_{11}, GPa	129	Modulus, E_f, GPa	367	Modulus, E_m, GPa	106
	Axial, E_{33}, GPa	192	Diameter, μm	142		
Poisson's ratio	ν_{13}	0.1905	Volume fraction	0.33		
	ν_{23}	0.2835				
Shear modulus	G_{13}, GPa	69.66				

Fiber Pushout Testing

The frictional properties of the interface were investigated using the fiber pushout test method. Pushout tests were performed on specimens in the as-received condition and specimens previously subjected to fatigue crack growth conditions.

Pushout testing of previously fatigued interfaces was performed in order to determine the actual frictional strength during crack bridging and to study the effect of relative fiber/matrix sliding on the integrity of the interface. Pushout samples with previously fatigued interfaces were obtained near the fracture surface of SEN and CCP specimens that exhibited crack bridging and failed during fatigue loading (Fig. 2).

Pushout specimens were prepared by sectioning with a thin diamond cut-off wheel to obtain slices approximately 1 mm thick. All samples were then polished on both surfaces to a 0.05-μm finish and final thicknesses ranging between 0.25 and 0.40 mm. The 143-μm-diameter fibers were pushed into a support plate with a 0.36-mm-wide groove using flat-bottomed tungsten carbide indenters. A displacement rate of 0.05 mm/min was used. The pushout data were recorded in a form of load versus time in conjunction with acoustic emissions to help identify

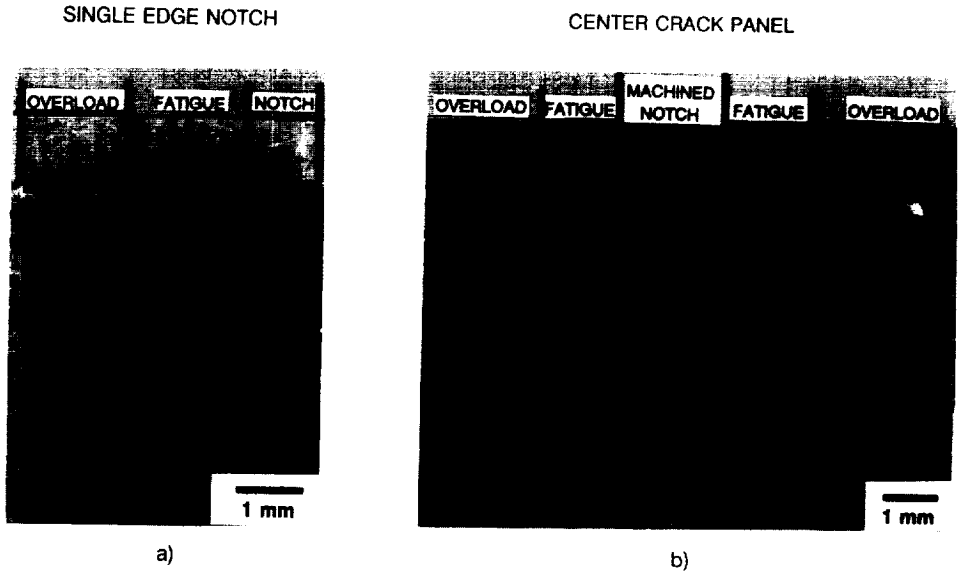

FIG. 2—*Failed fatigue crack growth specimens showing the approximate location of the slices taken for pushout testing:* (a) *SEN3 and* (b) *CCP3.*

the debond load. A more detailed description of the equipment and procedure can be found elsewhere [*15*]. A total of about 250 fibers were tested under the above described procedures.

In order to simulate the effect of relative fiber/matrix sliding that occurs at the interface during crack bridging, multiple reversed pushouts were performed. These pushouts were conducted on specimens in the as-received condition, with the fibers being pushed back and forth (about 10 to 20 μm) three or four times.

Fiber Testing

In order to determine the load carrying ability of bridging fibers and the effect of fiber/matrix sliding on the residual fiber strength, fiber tension testing was performed. Bridging fibers and fibers ahead of the crack tip were chemically removed from interrupted fatigue crack specimens that exhibited bridging. Fibers were extracted from both specimen geometries. The CCP specimen was cycled at $\Delta\sigma$ = 225 MPa for approximately one million cycles. The SEN specimen was loaded at $\Delta\sigma$ = 276 MPa for three million cycles. Fibers were also extracted from an interrupted SCS-6/Ti-15-3 double edge notch (DEN) specimen which was exposed to about one million cycles at $\Delta\sigma$ = 276 MPa. The bridging zone (a-a_0) was approximately 0.31, 0.35, and 0.87 mm for the CCP, SEN, and DEN specimens, respectively. Fibers were tested using a 5.0-mm gage length and a strain rate of 1.27 mm/min.

Analytical Modelling of Fiber Bridging

During crack bridging, the unbroken fibers in the bridged region carry part of the applied load. The effect of bridging fibers was modelled as a closure pressure on the crack wake using two different analytical techniques, the shear-lag model [*8*] and the fiber pressure model [*16*]. The shear-lag model relates the closure pressure, $c(x)$, to the crack opening displacement by assuming a constant interfacial frictional stress (τ_f) along a given debond length [*6*] for monotonic loading. The closure pressure was later modified to account for fatigue loading by relating the closure pressure ranges to the displacement ranges by (from Ref *8*)

$$\Delta c(x) = 2\sqrt{\frac{2\,\Delta u(x)\tau_f V_f^2 E_f E_c^2}{R(1 - V_f)^2 E_m^2}} \tag{1}$$

where

$\Delta c(x)$ = closure pressure ranges (as a function of position along the crack),
E_m = matrix modulus,
E_f = fiber modulus,
V_f = fiber volume fraction,
R = fiber radius,
τ_f = interfacial frictional shear strength, and
$\Delta u(x)$ = Half crack opening displacement ranges (as a function of position along the crack).

In the fiber pressure model, the closure pressure is related to the net tensile and/or bending stresses in the bridged area based on an elementary strength of materials approach. These stresses correspond to the load carried by the debonded fibers irrespective of the interface properties. The resulting closure profiles are given here for both specimen geometries

$$\text{SEN; } \Delta c(x) = \Delta\sigma^{\infty}\left(\frac{W}{W - a_0} + \frac{6Wa_0[0.5(W - a_0) - (x - a_0)]}{(W - a_0)^3}\right) \tag{2}$$

$$\text{CCP; } \Delta\sigma(x) = \Delta\sigma^{\infty}\left(\frac{W}{W - 2a_0}\right) \tag{3}$$

where $\Delta\sigma^{\infty}$ is the applied far-field stress range, a_0 is the initial notch, and W is the specimen width. A review of both analytical models can be found in Ref *17*.

Using both models, a finite element analysis was performed to determine the fatigue crack driving forces and crack opening displacements. For the shear lag model, the closure pressure was applied as a nonlinear foundation pressure. Since the closure pressure in the shear lag models was a function of the unknown crack opening displacements, an iterative scheme was required to solve for these unknown displacements. In the fiber pressure model, the closure pressure was applied simply as a pressure along the bridged area. For simplicity, the FEM analysis utilized an orthotropic homogeneous solution with composite effective properties. The composite stress intensity factor was determined using quarter point singularity elements at the crack tip. The details of the analytical procedure required to measure the closure corrected crack driving force and displacements is found elsewhere [*16*].

Results

Fatigue Crack Growth

The fatigue crack growth process was similar for both SEN and CCP crack geometries. In all cases fatigue cracks initiated readily at the machined notch root where fibers were damaged due to machining. The fibers that were partially cut during machining, if not already broken, usually failed during the first loading cycle. Since many fibers were damaged at the notch, many micro-cracks were initiated through the thickness of the composite. With additional fatigue cycling, these cracks coalesced to form a dominant crack. At times multiple cracks were observed to emanate from the notch. Multiple cracks were observed in both geometries; however, they were more common in the SEN geometry, probably due to the presence of greater bending.

It should be noted that even though fatigue cracks initiated readily, at stress ranges less than 150 MPa, fatigue cracks did not easily propagate into the matrix. At greater stresses, cracks propagated in the matrix, leaving fibers intact behind the crack tip.

Initially all cracks were bridged. Depending on the stress level, cracks that remained bridged were associated with decreasing crack growth rates and eventually crack arrest. When fibers in the crack wake started failing, the crack growth rates accelerated. The remote applied stress for which the specimens eventually exhibited fiber failure was greater than 180 MPa for the SEN geometry and 225 MPa for the CCP geometry.

The fatigue crack growth rates for the tested specimens as a function of the applied stress intensity factor ΔK_{app} are shown in Fig. 3. The crack that remained fully bridged resulted in crack arrest, while the FCG rates of specimens exhibiting some fiber failure were typically higher than those of bridged cracks, but still lower than those of the unreinforced matrix (see Fig. 3). However, as unbridged cracks propagated further in the specimen, fiber failures were observed to occur ahead of the crack tip.

Fractography

The fracture surfaces of both specimens geometries are shown in Fig. 4. As seen on the fracture surface, very little fiber pullout was observed. Fiber failures typically occurred within 1 to 2 fiber diameters from the fracture surface. In the fatigue region, extensive damage was observed in the fiber/matrix interface. In the overload region, however, interfaces were not

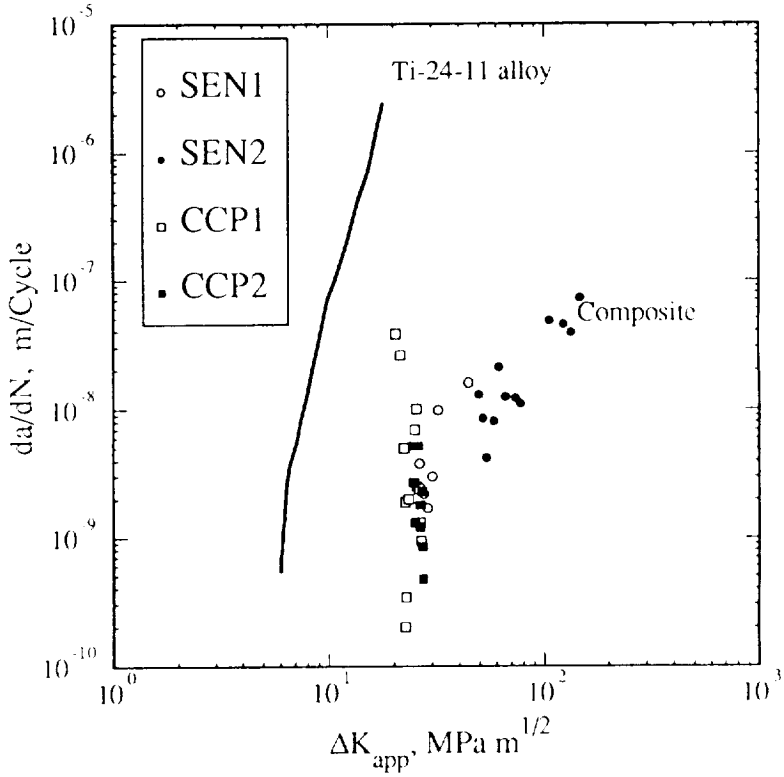

FIG. 3 *Composite fatigue crack growth rates as a function of the applied* ΔK_{app} *in comparison to matrix data.*

damaged. Furthermore, the fracture surface in the fatigue region was littered with debris, presumably from the damaged interfaces and fibers. Again, debris was not observed in the overload region. Interfacial fretting was also observed during fatigue crack growth on the surface of a specimen containing fibers which were partially exposed from polishing (Fig. 5). As seen in Fig. 5, interfacial debris has been ejected from the interface. Interfacial failure in this composite occurred between the carbon coatings on the SCS-6 fiber. These coatings contain weak graphitic phases [*18*] which seem prone to wear during fatigue.

Interface Damage Zone Measurements

In order to determine the extent of interfacial damage, interrupted fatigue crack growth specimens were chemically etched to expose the fibers. Figure 6 shows typical damage observed on the interfaces of fatigued fibers. Interfacial damage was never observed in fibers outside the fatigue crack growth region. Similar debond zones were observed with the scanning acoustic microscope (Fig. 7). The extent of interfacial damage is shown in Fig. 8 for both crack geometries. As shown in Fig. 8, the observed damage zones are greater for fibers near the machined notch in comparison to fibers closer to the crack tip.

By assuming the measured damage zones represent the actual debond length *l*, the interfacial

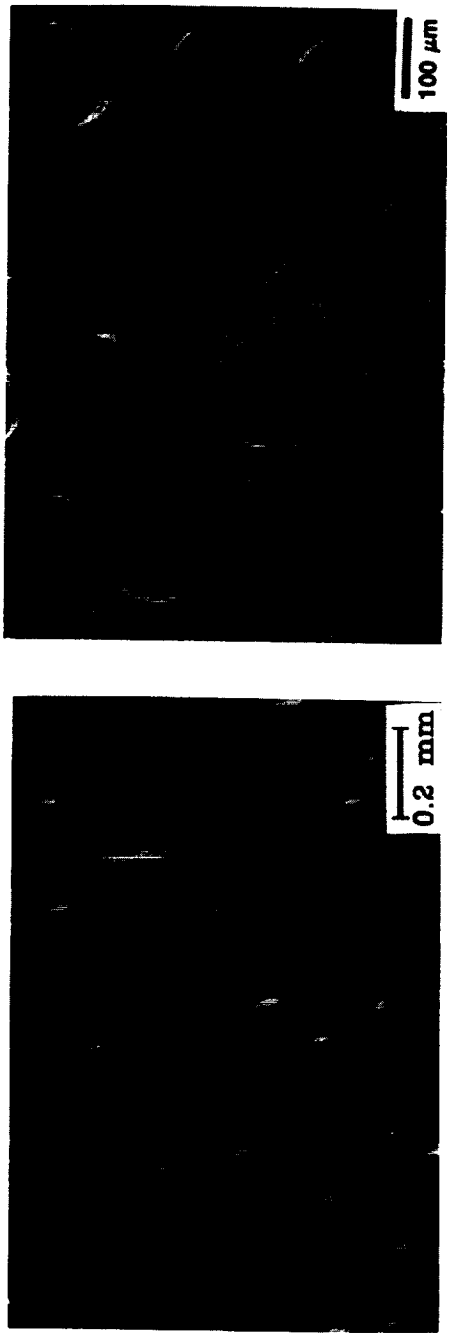

FIG. 4—*Typical micrographs of the fracture surface for:* (a) *SEN and* (b) *CCP.*

FIG. 5—*Micrograph of a partially exposed fiber showing inter-facial debris (SEN5).*

friction strength can be determined using a shear-lag approach. The relation between l and τ_i, as given by McCartney [7] is

$$l(x) = \sqrt{\frac{u(x)R(1 - V_f)E_fE_m}{\tau_iE_c}} \tag{4}$$

where $l(x)$ is the debond length and $u(x)$ is the crack opening displacement at a given location x. Using the experimentally determined debond lengths and CODs in conjunction with Eq 4, an average friction strength of 23 and 34 MPa were calculated for the CCP and SEN geometries, respectively.

Pushout Testing

As-received condition—A typical pushout response of specimens in the as-received condition is shown in Fig. 9. The debonding event (P_d) coincides with a load drop and pronounced acoustic emissions. Debonding is followed by a gradual decrease in the load as the fiber is displaced. At this point the only resistance to the fiber displacement comes

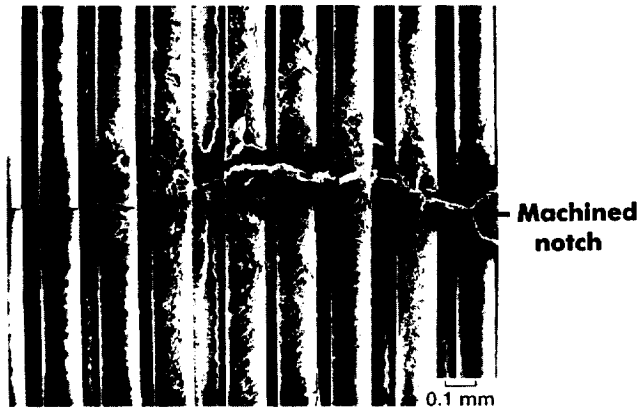

FIG. 6—*Interfacial damage exposed by dissolving the matrix.*

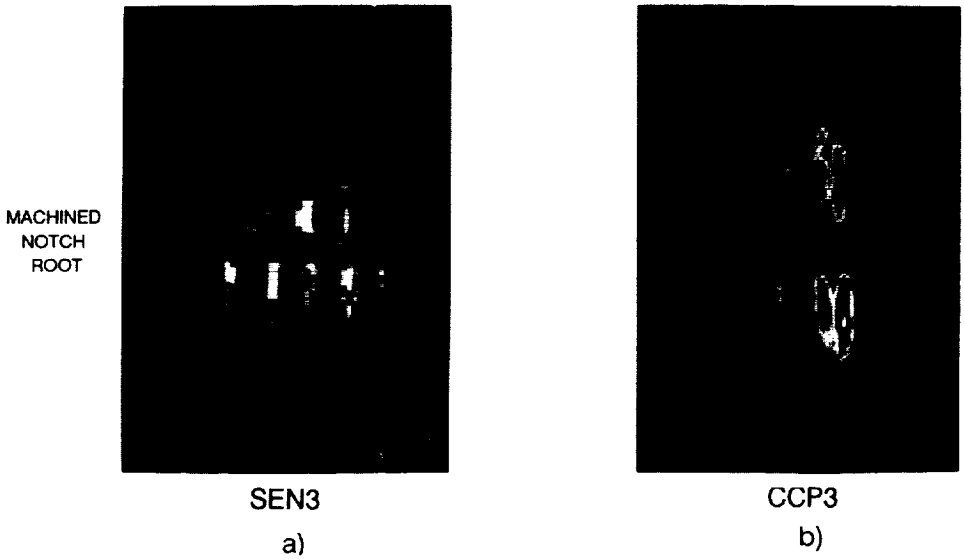

FIG. 7—*Interfacial damage zones as observed by scanning acoustic microscopy for:* (a) *SEN3 and* (b) *CCP3 specimens.*

from the frictional shear stresses at the interface. The load immediately after debonding P_l is considered to be the load needed to overcome friction. The interfacial debond shear stress for the as-received composite was determined to be 122 MPa using a simple force balance (i.e., $\tau_d = P_d/2\pi Rl$). Likewise, the frictional shear stress was calculated to be 75 MPa. The frictional strength derived from the debond zone measurements (τ_f ave. = 28

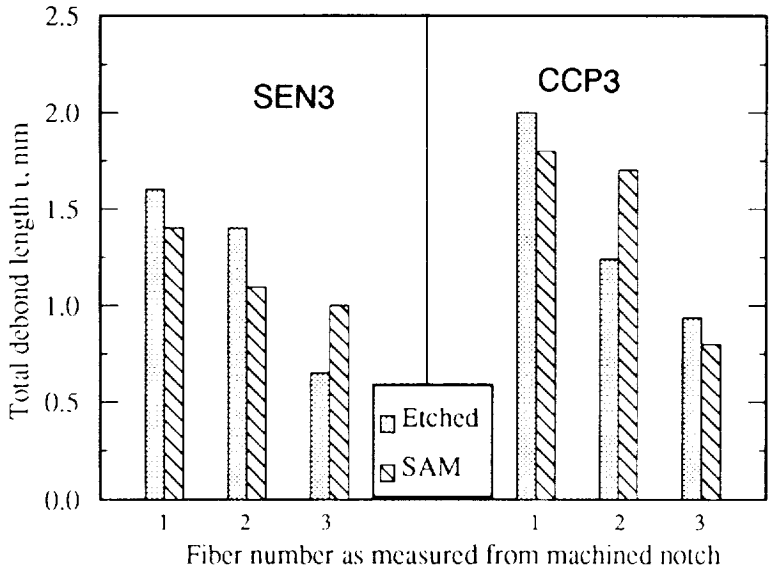

FIG. 8—*Measured interfacial damage zones.*

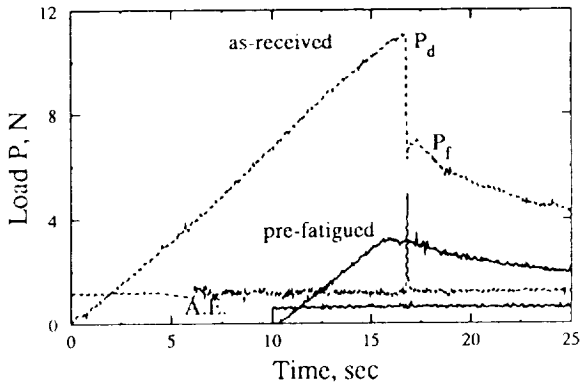

FIG. 9—*Typical pushout response of interfaces in the as-received and pre-fatigued conditions.*

MPa) is significantly lower than the as-received friction strength of τ_i = 75 MPa. This may be attributed to interfacial damage incurred during fatigue sliding.

Previously Fatigued Interfaces—The effect of relative fiber/matrix sliding during crack bridging on the interfacial friction strength, as determined by pushout testing, is shown in Fig. 9 in comparison to the as-received response. The response of the pre-fatigued specimen clearly suggests that these interfaces were already debonded since no load drop or acoustic emission events were observed. The measured average interfacial friction strength of previously fatigued interfaces was calculated to be 32 ± 10 MPa for the SEN specimen and approximately 45 MPa for the CCP specimen. Compared with as-received interfacial frictional strength, this represents about a 57 and 40% decrease in friction strength for the SEN and CCP, respectively. These values are in better agreement with those calculated from the debond zone measurements.

Multiple Reverse Pushout Testing—Multiple reversed pushouts were performed on the as-received specimens in order to simulate the effect of fatigue on the interfacial shear strength. The fibers were typically displaced 10 to 20 μm. The first pushout shows behavior typical of as-received material with a bonded interface (Table 3). Subsequent pushouts show a steady decrease in the frictional resistance of the interface with increasing cycles. After only four pushouts, the frictional shear stress has decreased to 39 ± 7 MPa, which is in the order of the frictional shear strength measured near the fracture surface (see Table 3) of pre-fatigued specimens.

Fiber Tension Testing

Since extensive damage was observed for interfaces that were subjected to cyclic loading, tension testing was performed on bridging fibers to determine the effect of this damage on fiber strength. The results are shown in Fig. 10. The tensile strength of bridging fibers in the CCP specimen was 3530 ± 146 MPa. In comparison, the tensile strength of fibers ahead of the crack tip was 4282 ± 212 MPa. The tensile strength of bridging fibers in the SEN specimen was 3720 ± 480 MPa in comparison to 4150 ± 340 MPa for nonbridging fibers, an insignificant difference for all practical purposes. In the SCS-6/Ti-15-3 DEN specimen, however, bridging fibers near the notch had an average tensile strength of 2664 ± 514 MPa. Fibers near the crack tip, which were subjected to lower fiber/matrix displacements, had an average tensile strength of 3430 ± 286 MPa. Fibers ahead of the crack tip, whose interfaces were not subjected to

TABLE 3—*Interfacial friction strength results from pushout tests and debond length measurements.*

Test Conditions	Type of Technique	Friction Strength, τ_i, MPa
As-received	Pushout	75 ± 6
Fatigue crack growth specimen CCP	Debond lengths	23
	Pushout	45
Fatigue crack growth specimen SEN	Debond lengths	34
	Pushout	32
Multiple reverse pushouts	Initial push	75 ± 6
	Second push	55 ± 6
	Third push	48 ± 8
	Fourth push	39 ± 7

relative fiber/matrix sliding, were significantly stronger with average tensile strength of 4415 ± 684 MPa. The guaranteed minimum strength of the virgin SCS-6 fibers by the manufacturer is 3490 MPa.

Crack Opening Displacement

Measurements of the crack opening displacements (COD) were obtained using the SEM loading stage. Measurements were typically made starting at the root of the machined notch and ending at the crack tip. Typical COD profiles at maximum and minimum loads, shown in Fig. 11, indicate that fatigue cracks remain propped open at minimum load. The displacements at minimum load are usually about half the maximum displacements even though the R ratio was 0.1.

Both the fiber pressure model and shear-lag model were used to predict the ΔCODs during crack bridging. Figure 12 shows the ΔCODs predicted by the fiber pressure model in comparison with experimentally obtained ΔCODs for a variety of crack lengths and applied loads. For the most part, the fiber pressure model predicted the ΔCOD profiles well. Also shown for

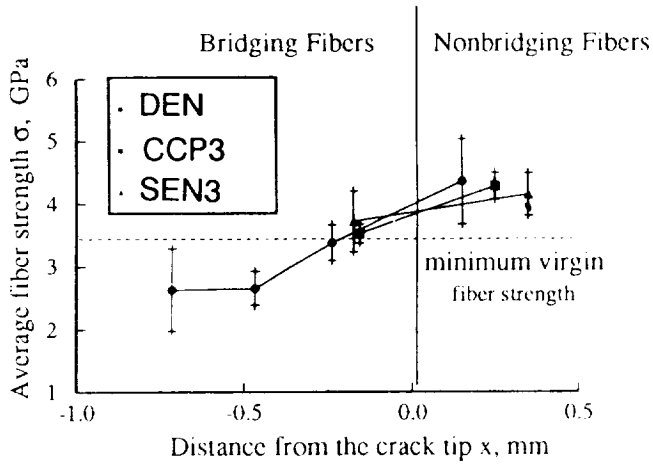

FIG. 10—*Extracted SCS-6 fiber strength values for bridging and nonbridging fibers.*

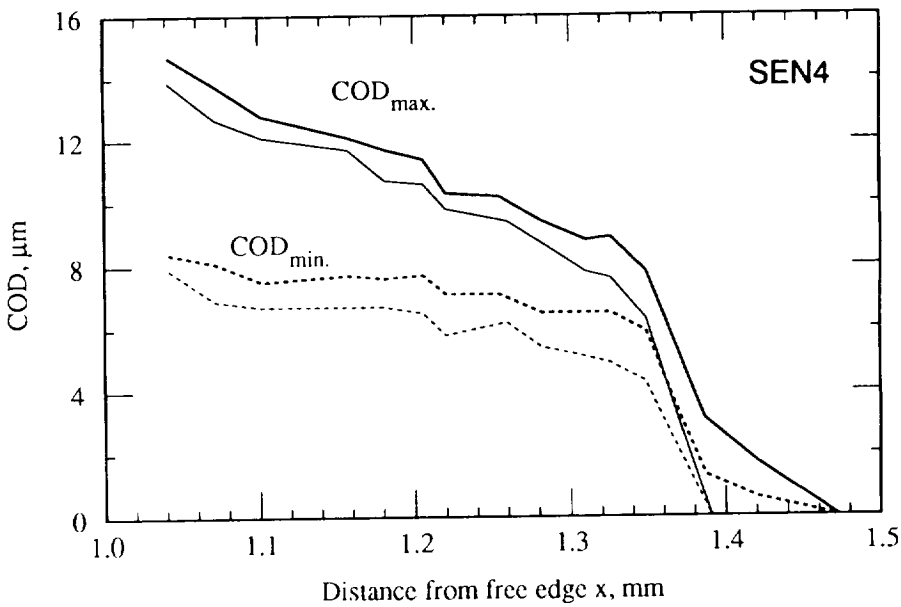

a) SEN

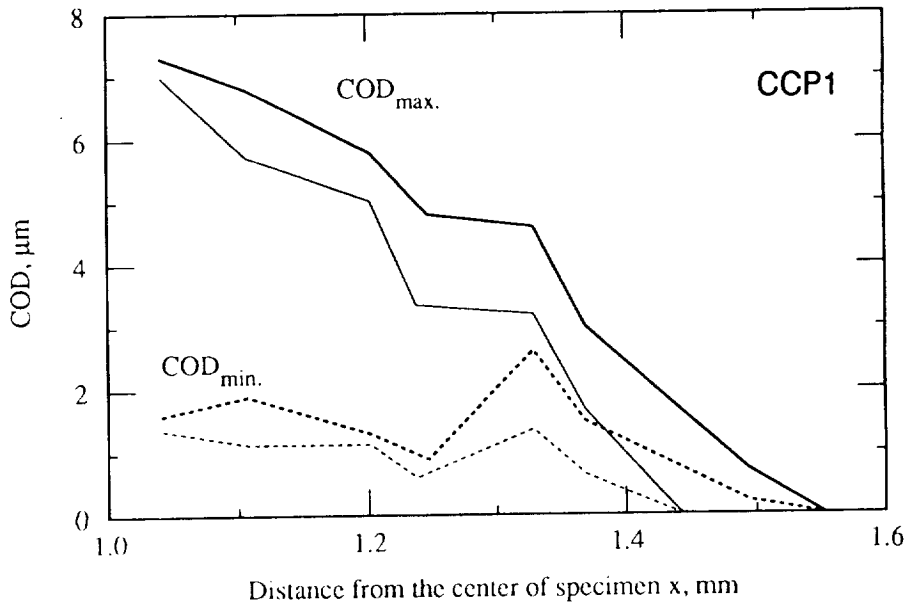

b) CCP

FIG. 11—*Measured crack opening displacements at maximum and minimum loads for:* (a) *SEN4 and* (b) *CCP1.*

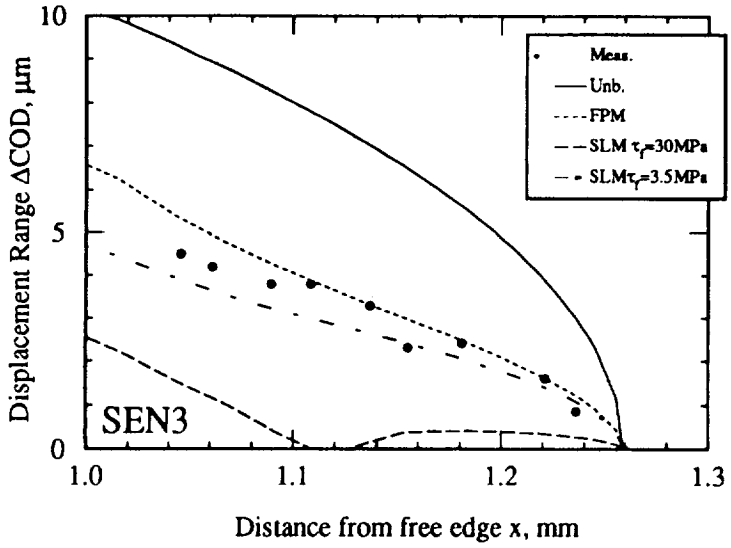

a) SEN

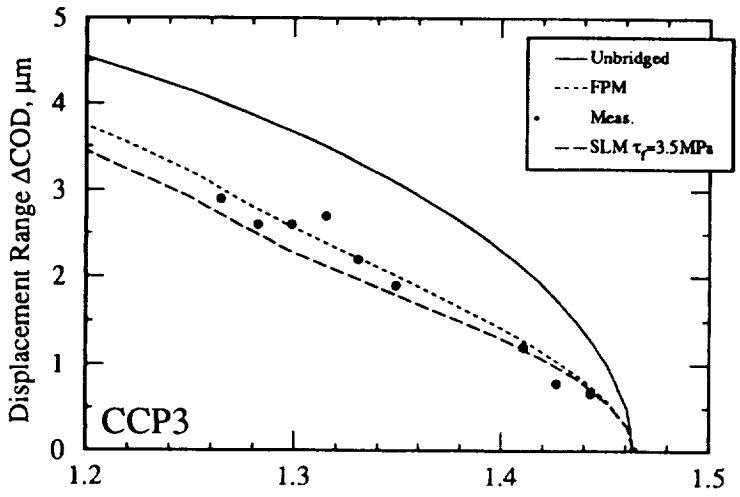

b) CCP

FIG. 12—*Predicted crack opening displacement ranges in comparison to measured values for:* (a) *SEN and* (b) *CCP.*

comparison are the expected ΔCODs for unbridged cracks. As seen in Fig. 12, the measured ΔCODs of bridged cracks are much smaller than the predicted ΔCODs of unbridged cracks.

Predicting the ΔCOD profiles with the shear-lag model requires knowledge of the interfacial friction strength. As a first approximation τ_i = 30 MPa was used based on the pushout results. However, as shown in Fig. 12*a*, the ΔCOD profiles predicted with τ_i = 30 MPa were typically smaller than the measured values. By varying τ_i, it was determined that τ_i = 3.5 MPa generally resulted in good correlation between the observed and predicted ΔCODs for both crack geometries (see Fig. 12).

Even though the predicted ΔCOD profiles using τ_i = 3.5 MPa generally resulted in good correlation with the experimentally measured crack profiles, some inconsistencies were observed. For example, near the crack tip, the shear lag based predictions of the ΔCODs were usually larger than experimental measurements (Fig. 13). This implies that the interfacial friction strength is greater than τ_i = 3.5 MPa near the crack tip. This scenario was modeled by varying τ_i along the crack wake until good agreement with the measured displacements was achieved. As shown in Fig. 13*b*, for the CCP geometry, by varying the interfacial friction strength along the bridged zone, it was determined that a combination of τ_i = 1 MPa near the notch and τ_i = 30 MPa near the crack tip resulted in good agreement for the entire crack profile. For the SEN geometry (Fig. 13*a*), however, a combination of τ_i = 3 MPa near the notch and τ_i = 10 MPa near the crack tip resulted in the best correlation.

Fatigue Crack Driving Force During Crack Bridging

The two models were also used to account for the reduction in the effective crack driving force (ΔK_{eff}), Ref *16*, due to fiber bridging. As shown in Fig. 14, both models predict significantly lower effective fatigue crack driving forces during crack bridging in comparison to an unbridged crack. Furthermore, ΔK_{eff} decreases as the crack length increases. This correlates well with the observed decrease in fatigue crack growth rates before fiber failure.

Since fatigue crack growth during bridging occurs only in the matrix, the composite fatigue crack growth rates were compared to those of the unreinforced Ti-24-11 matrix utilizing the ΔK_{eff} predicted by the models (Fig. 15). As seen in Fig. 15*a*, the effective crack driving force predicted by the fiber pressure model shifts the composite crack growth rates in good agreement with the unreinforced matrix.

The shear lag model with a constant interfacial friction strength of 3.5 MPa substantially overpredicted the composite crack driving force as shown in Fig. 15*b*. However when the τ_i was varied along the crack wake in agreement with the measured ΔCODs, the shear lag calculated ΔK_{eff} brought the composite data in closer agreement with the unreinforced matrix data (see Fig. 15*c*). As also shown, the shear lag model predicts the crack driving force much better for the CCP geometry than the SEN geometry.

Discussion

The results of this study show that relative fiber/matrix sliding during fatigue results in interfacial damage. Interfacial wear degrades the mechanical properties of the interface and fiber which influence the fatigue crack driving force.

Interfacial Properties

Interfacial damage was readily observed on the fracture surface of fatigue specimens and on the interfaces of interrupted specimens. The interfacial damage observed consisted mostly of cracks and spalling in the carbon-rich coatings of the SCS-6 fiber. The damage zones were

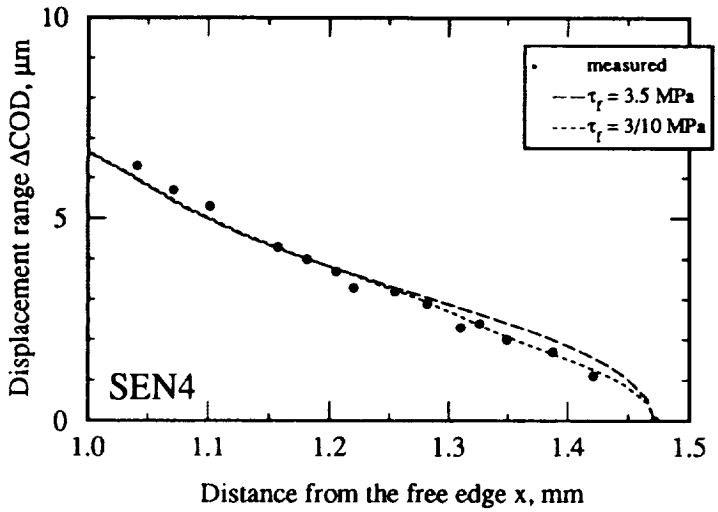

a) SEN

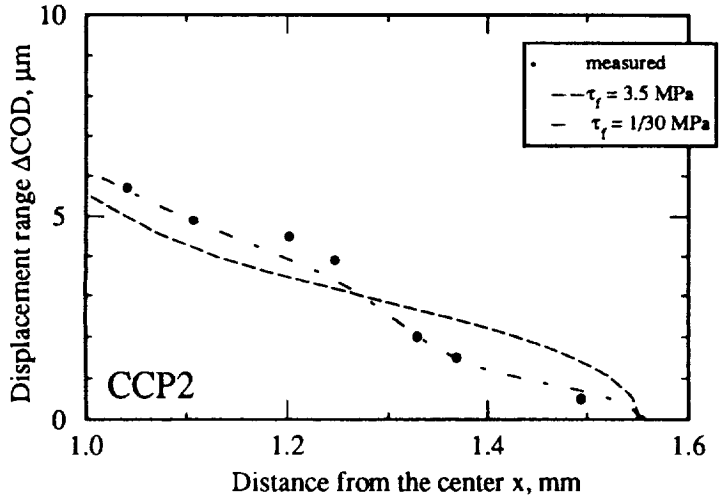

b) CCP

FIG. 13—*Calibration of the SLM with a variable interfacial friction stress for:* (a) *SEN and* (b) *CCP specimens.*

typically in the order of 1 to 2 mm long. Pushout testing of previously fatigued specimens suggest that interfacial damage incurred during fatigue results in drastic deterioration of the frictional properties of the interface. All the factors governing the extent and magnitude of interfacial degradation are not clear at this time; however, multiple reversed fiber pushout testing suggests that interfacial damage can occur very rapidly during fatigue, and maybe as a function of relative fiber/matrix sliding distance (see Table 3).

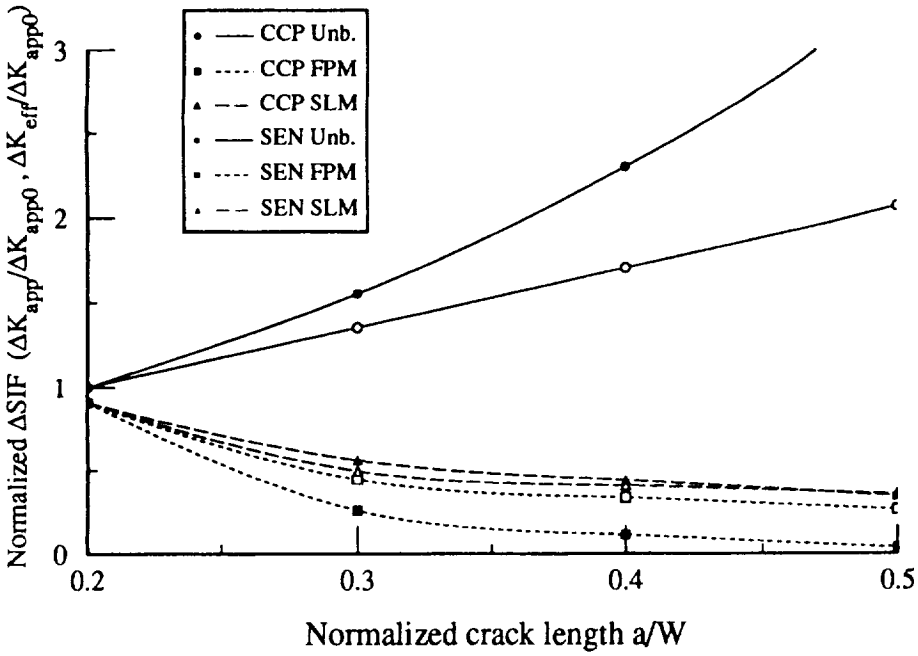

FIG. 14—*Effective normalized stress intensity factors as a function of the crack length, where* K_{appo} *is the applied SIF at the initial crack length* a_o.

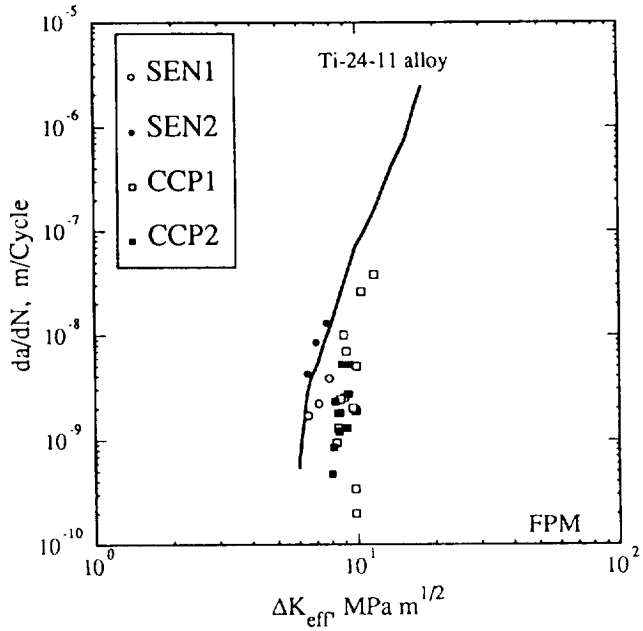

a) FPM

FIG. 15—*Composite crack growth rates plotted as a function of* ΔK_{eff} *in comparison to the matrix data using:* (a) *FPM,* (b) *SLM with constant* τ_t = *3.5 MPa, and* (c) *SLM with a variable* τ_t.

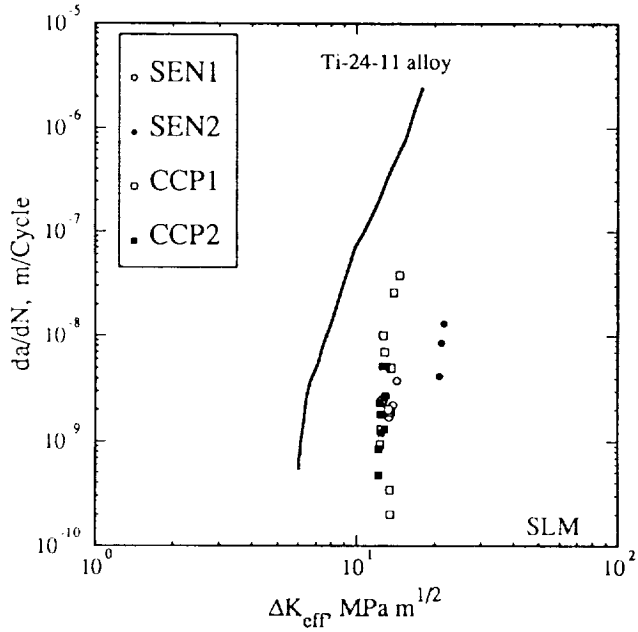

b) SLM τ_f= 3.5 MPa

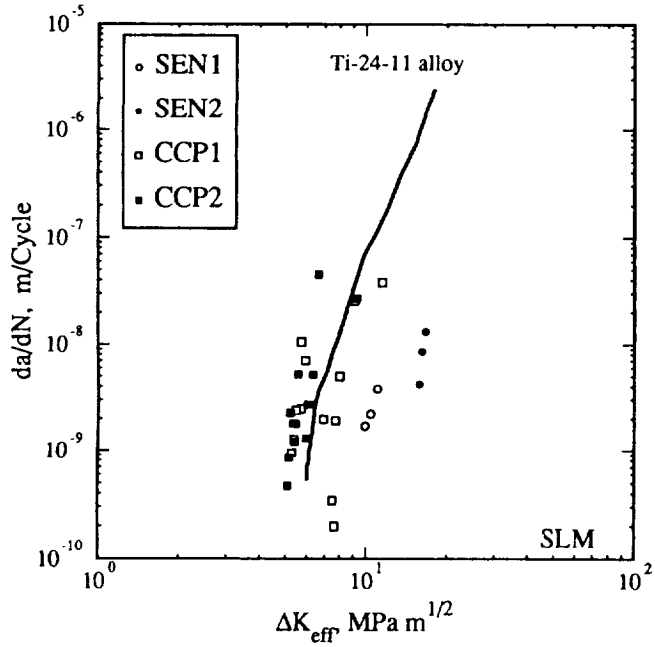

c) SLM variable τ_f

FIG. 15—*Continued.*

Three different methods were used to ascertain the interfacial properties of the bridging fibers. Both pushout testing of the fibers in the bridging zone and debond length measurements resulted in an estimated τ_i of 20 to 30 MPa (as compared to τ_i of 75 MPa for the as-received composite). However, the τ_i which best fit the ΔCOD measurements, from the shear lag model, suggested that the shear strength varies within the crack wake. For the largest portion of the bridged zone, a low τ_i of 1 to 3 MPa fit the measured ΔCODs; however, near the crack tip, a τ_i of 10 to 30 MPa (depending on specimen geometry) was needed to fit the measured displacements.

The discrepancies in the τ_i values calculated through the different methods may be due to several factors. Even though $\tau_i = 1 \sim 3$ MPa obtained from ΔCOD measurements seems considerably lower than the interfacial friction strength observed during pushout testing, it should be noted that the pushout values were obtained at depths approximately 1 mm from the fracture surface. Fractographic examination of the interface revealed that the greatest damage is near the vicinity of the crack plane. The τ_i values obtained from the ΔCOD measurements therefore might reflect the interface conditions near the crack plane.

Fiber Strength

Interfacial wear in the crack wake also resulted in degradation of the tensile strength of the bridging fibers. As seen in Fig. 10, the reduction in the fiber strength was significantly smaller for fibers obtained from the SEN and CCP SCS-6/Ti-24-11 specimens than the fibers obtained from the DEN SCS-6/Ti-15-3 specimen. Furthermore, for the DEN specimen, the strength of bridging fibers increased near the crack tip. Fibers near the crack tip were subjected to lower relative fiber/matrix displacements and displayed smaller damage zones. Fibers ahead of the crack tip, whose interfaces were not subjected to relative fiber/matrix sliding, did not display any interfacial damage and were significantly stronger.

It is not clear why a greater loss in fiber strength was observed in the DEN SCS-6/Ti-15-3 specimen. This phenomenon may be related to a difference in the chemistry of the reaction zones or bonding of the interface between the two matrix alloys. However, comparison of the fiber surfaces revealed that the fibers extracted from the DEN specimen exhibited more damage. As shown earlier by the multiple pushout test method, the relative magnitude of fiber/matrix sliding influences the extent of interfacial damage.

Comparing the ΔCODs of these specimens, certain trends became evident. The ΔCODs for the SEN and CCP specimen were in the order of 4 μm, while the ΔCODs for the DEN specimen were approximately 11 μm at the machine notch. Furthermore, for the DEN geometry, in the case of fibers near the crack tip whose strength did not degrade significantly (3430 $\pm$ 286 MPa), the relative ΔCODs were also in the 4-μm range. The strength of these fibers correlates well with the fiber strengths observed in the bridging fibers of the SEN (3720 $\pm$ 480 MPa) and CCP (3530 $\pm$ 146 MPa) geometries. This suggests that interfacial damage and degradation of the fiber strength during bridging is more likely in the presence of large ΔCODs. Furthermore, damaged fibers extracted from the bridged region typically failed within the damage zone, whereas undamaged fibers ahead of the crack tip typically failed anywhere within the gage section and many times outside the gage. Since the damage is greater near the fracture surface, this explains why little pullout was observed (in the order of 1 to 2 d_f), even though the damage zones were significantly larger ($\simeq$10 d_f).

Modelling of the Bridging Process

The shear lag model is predicted on the ability to accurately describe the load transfer from the cracked matrix to the bridging fibers through an interfacial sliding process. As the present

study has shown, the interfacial wear process is very complex, resulting in a nonuniform interfacial damage as a function of the distance from the crack tip and the distance from the crack plane for a given fiber/matrix interface. This nonuniformity of the interfacial damage results in a variable frictional shear strength along the crack wake.

Typical application of the shear lag model assumes a single τ_f value in the analysis. However, due to the factors described above, the use of a single τ_f resulted in the shear lag model overestimating the effective crack driving force, as shown in Fig. 15*b*. When the analysis was performed using a variable τ_f (the same combination of τ_f as previously used in predicting the ΔCODs, Fig. 13), the shear lag model brought the composite FCG data much closer in agreement with the unreinforced matrix data as shown in Fig. 15*c*. Unfortunately, obtaining a single accurate estimate of τ_f is in itself problematic; the need to establish different τ_f values for varied locations within the crack wake further complicates the shear lag modelling process.

While most of the discussion has dealt with the shear lag model, the success of the fiber pressure model in predicting both the measured crack opening displacements and the effective fatigue crack driving forces (Figs. 12 and 15*a*) should be emphasized. This rather straightforward approach in calculating the closure pressure function seems adequate in predicting the effect of bridging.

Interestingly enough, the FPM and the SLM with variable τ_f predict the trends observed during bridging even though the two closure pressures are derived quite differently. Figure 16 shows closure pressure profiles calculated from both models. The closure pressure profile for the fiber pressure model is a function of the crack geometry and applied load. For the CCP geometry the closure pressure profile is constant over the entire bridged region. In the SEN geometry, the presence of bending generally results in greater closure pressure profiles. Bending also results in a slightly decreasing closure pressure profile along the bridging zone (higher near the notch and lower near the crack tip).

In the shear lag model, the closure pressure depends on the interfacial friction strength and crack opening displacements. This is evident by the closure pressure profile, which decreases to zero at the crack tip. In comparison, the fiber pressure model predicts much higher closure pressures near the crack tip. The difference in closure pressure profiles explains why the fiber pressure model typically predicts lower ΔCODs and ΔK_{eff}s in comparison with the shear lag model.

Varying the interfacial friction stress to reflect damaged interfaces also changes the closure pressure profile. As shown in Fig. 16, this results in higher fiber stress near the crack tip. This modification results in a closure pressure profile which is similar to that predicted by the fiber pressure model. Therefore, the FPM fortuitously predicts a closure pressure profile consistent with the observed mechanisms during bridging. Even though the fiber pressure model is not always consistent in predicting the overall ΔCODs, it does seem to predict realistic crack driving forces. This also suggests that the crack driving force during bridging is most sensitive to the closure pressure and ΔCODs near the crack tip rather than the overall crack profile.

Finally, before either of these models can be used to predict fatigue life, it is necessary for these models to accurately predict the onset of fiber failure. This issue will be addressed in future work.

Conclusions

1. The fatigue crack growth process of a unidirectionally reinforced SCS-6/Ti-24Al-11Nb intermetallic matrix composite was studied using a fatigue loading stage mounted inside a scanning electron microscope. The composite exhibited FCG rates orders of magnitude lower than its unreinforced matrix. The decrease in the FCG rates was caused by crack tip shielding resulting from unbroken fibers bridging the crack wake.

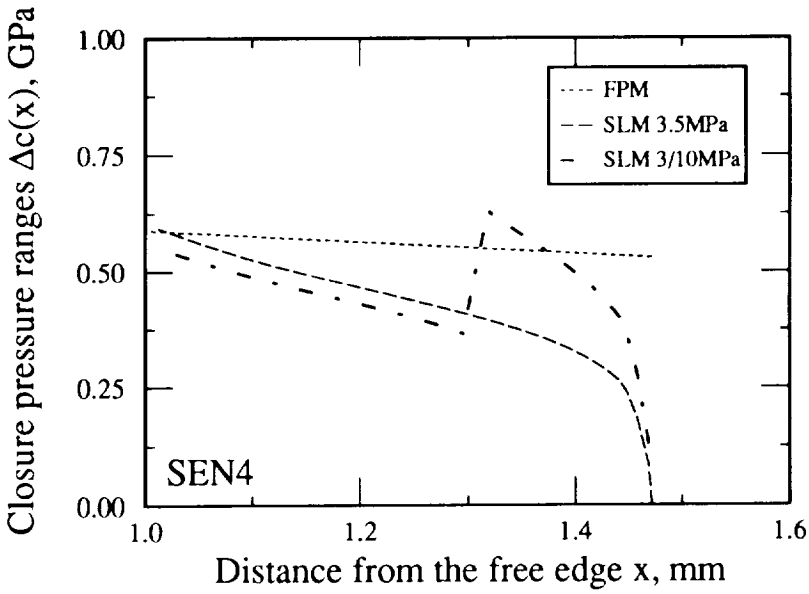

a) SEN

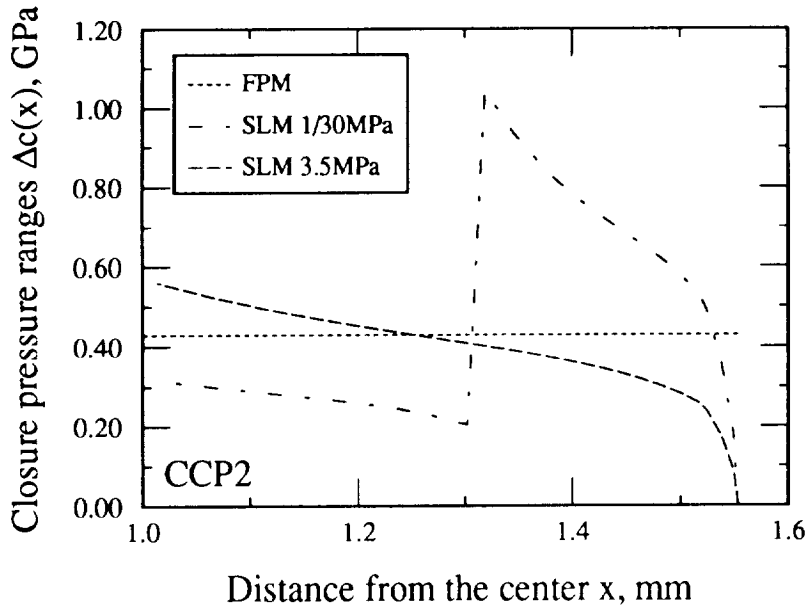

b) CCP

FIG. 16—*Comparison of the closure pressure ranges from the FPM and SLM for:* (a) *SEN and* (b) *CCP.*

2. Interfacial damage in the bridging fibers, induced by relative fiber/matrix sliding, was found to occur in the crack wake of the tested specimens subjected to fatigue crack growth conditions. The interfacial friction shear strength measured in the crack wake using pushout testing revealed lower values than the as-received interface. The degree of interfacial damage was not uniform along the bridged crack wake. Higher damage zones were observed near the machined notch in comparison to the crack tip.

3. The interfacial wear also reduced the fiber strength of the bridging fibers. The reduction in the fiber strength was found to depend on specimen geometry and is thought to increase as a function of the magnitude of relative fiber/matrix displacements.

4. Two different fiber bridging models were used in an attempt to predict the influence of bridging on the fatigue crack driving force in composites. The shear lag model required a variable τ_f in the crack wake before its predictions agreed with the trends exhibited by the experimental data. The fiber pressure model, however, did an excellent job in predicting both the FCG data and the ΔCOD in the bridged zone even though it does not require a knowledge of τ_f.

Acknowledgments

The authors would like to thank Ken Wright and GEAE for providing the material tested. Special thanks is also extended to Rich Klaassen of GE Aircraft Engine-Quality Technology Center for his SAM contribution to this study.

References

[1] Kantzos, P., Telesman, J., and Ghosn, L. J., "Fatigue Crack Growth in a Unidirectional SCS-6/Ti-15-3 Composite," *Composite Materials: Fatigue and Fracture (3rd Vol.), ASTM STP 1110*, T. K. O'Brian, Ed., ASTM, Philadelphia, 1991, pp. 711–731.

[2] Sensmeier, M. D. and Wright P. K., "The Effect of Fiber Bridging on Fatigue Crack Growth in Titanium Matrix Composite," *Proceedings*, Fundamental Relationships Between Microstructures and Mechanical Properties of Metal Matrix Composites, P. K. Liaw et al., Ed., The Minerals, Metals, and Materials Society, Warrendale, PA, 1990, pp. 441–457.

[3] Bakuckas, J. G. and Johnson, W. S., "Application of Fiber Bridging to Fatigue Crack Growth in Unidirectional Titanium Matrix Composites," *Journal of Composites Technology and Research*, Vol. 15, No. 3, Fall 1993, pp. 242–255.

[4] Walls, D., Bao, G., and Zok, F., "Fatigue Crack Growth in a Ti/SiC Composite," *Mechanical Fatigue of Advanced Materials*, R. O. Ritchie, R. H. Dauskart, and B. N. Cox, Eds., MCEP, Birmingham, UK, 1991, pp. 343–356.

[5] Davidson, D. L., "The Micromechanics of Fatigue Crack Growth at 25°C in Ti-6Al-4V Reinforced with SCS-6 Fibers," *Metallurgical Transactions A*, Vol. 23A, 1992, pp. 865–879.

[6] Marshall, D. B., Cox, B. N., and Evans, A. G., "The Mechanics of Matrix Cracking in Brittle-Matrix Fiber Composites," *Acta Metallurgica*, Vol. 33, 1985, pp. 2013–2021.

[7] McCartney, L. N., "Mechanics of Matrix Cracking in Brittle-Matrix Fiber-Reinforced Composites," *Proceedings of the Royal Society of London, Series A*, Vol. 409, 1987, pp. 329–350.

[8] McMeeking, R. M. and Evans, A. G., "Matrix Fatigue Cracking in Fiber Composites," *Mechanics of Materials*, Vol. 9, 1990, pp. 217–227.

[9] Kantzos, P., Eldridge, J. I., Koss, D., and Ghosn, L. J., "The Effect of Fatigue on the Interfacial Friction Properties of SCS-6/Ti-15-3 Composites," in *Advanced High-Temperature Engine Materials Technology Program*, Proceedings of the 4th Annual HITEMP Review, NASA CP 10082, October 1991, pp. 36-1 to 36-11.

[10] Marshall, D. B., Shaw, M. C., and Morris, W. L., "Measurement of Interfacial Debonding and Sliding Resistance in Fiber Reinforced Intermetallics," *Acta Metallurgica et Materialla*, Vol. 40, No. 3, 1992, pp. 443–454.

[11] Warren, P. D., Mackin, T. J., and Evans, A. G., "Design, Analysis and Applications of an Improved Push-Through Test for the Measurement of Interface Properties in Composites," *Acta Metallurgica et Materialla*, Vol. 40, No. 6, 1992, pp. 1243–1249.

[12] Telesman, J., Kantzos, P., and Brewer, D., "In Situ Fatigue Loading Stage Inside Scanning Electron Microscope," Lewis Structures Technology—1988, NASA CP3003, Vol. 3, May 1988, pp. 161–172.

[13] Gilmore, R. S., Hewes, R. A., Thomas, L. J., III, and Young, J. D., "Broad Band Acoustic Microscopy: Scanned Images with Amplitude and Velocity Information," *Acoustical Imaging*, Vol. 17, 1989, pp. 97–110.

[14] Klaassen, R., "Internal Structural Characterization," G.E. Aircraft Interim Report No. 6 for WPAFB Contract No. F33615-88-C-5433, Project No. 2418/02, 15 Jan. 1992.

[15] Eldridge, J. I., Bhatt, R. T., and Kiser, J. D., "Investigation Interfacial Shear Strength in SiC/Si_3N_4 Composites," *Ceramic Engineering and Science Proceedings*, Vol. 12, *Proceedings*, 15th Annual Conference on Composites and Advanced Ceramic Materials, 1991, pp. 1152–1171.

[16] Ghosn, L. J., Kantzos, P., and Telesman, J., "Modeling of Crack Bridging in a Unidirectional Metal Matrix Composite," *International Journal of Fracture*, Vol. 54, 1992, pp. 345–357.

[17] Telesman, J., Ghosn, L. J., and Kantzos, P., "Methodology for Prediction of Fiber Bridging Effects in Composites," *ASTM Journal of Composites Technology and Research*, Vol. 15, No. 3, Fall 1993, pp. 234–241.

[18] Ning, X. J., Pirouz, P., Lagerlof, K. P. D., and DiCarlo, J., "The Structure of Carbon in Chemically Vapor Deposited SiC Monofilaments," *Journal of Material Research*, Vol. 5, No. 12, December 1990, pp. 2865–2876.